Article

Biotin Decorated Gold Nanoparticles for Targeted Delivery of a Smart-linked Anticancer Active Copper Complex: In Vitro and In Vivo Studies

Anup Kumar Pramanik, * Siddikuzzaman, Duraippandi Palanimuthu, Kumaravel Somasundaram, and Ashoka Gnanadoss Samuelson

Bioconjugate Chem., **Just Accepted Manuscript** • DOI: 10.1021/acs.bioconjchem.6b00537 • Publication Date (Web): 21 Nov 2016

Biotin Decorated Gold Nanoparticles for Targeted Delivery of a Smart-linked Anticancer Active Copper Complex: *In Vitro* and *In Vivo* Studies

Anup K. Pramanik[†], Siddikuzzaman[‡], Duraippandi Palanimuthu[†], Kumaravel Somasundaram*[‡] and Ashoka G. Samuelson*[†]

[†]*Department of Inorganic and Physical Chemistry,* [‡]*Department of Microbiology and Cell Biology, Indian Institute of Science, Bangalore- 560012, India*

Abstract: The synthesis and anticancer activity of a copper(II) diacetyl-bis(N4-methylthiosemicarbazone) complex and its nanoconjugates are reported. The copper(II) complex is connected to a carboxylic acid group through a cleavable disulfide link to enable smart delivery. The copper complex is tethered to highly water soluble 20 nm gold nanoparticles (AuNPs), stabilized by amine terminated lipoic acid-polyethylene glycol (PEG). The gold nanoparticle carrier was further decorated with biotin to achieve targeted action. The copper complex and the conjugates with and without biotin, were tested against HeLa and HaCaT cells. They show very good anticancer activity against HeLa cells, a cell line derived from cervical cancer and are less active against HaCaT cells. Slow and sustained release of the complex from conjugates is demonstrated through cleavage of disulphide linker in the presence of glutathione (GSH), a reducing agent intrinsically present in high concentrations within cancer cells. Biotin appended conjugates do not show greater activity than conjugates without biotin against HeLa cells. This is consistent with drug uptake studies which suggests similar uptake profiles for both conjugates *in vitro*. However, *in vivo* studies using a HeLa cell xenograft tumor model shows 3.8 fold reduction in tumor volume for the biotin conjugated nanoparticle compared to the control whereas the conjugate without biotin shows only 2.3 fold reduction in the tumor volume suggesting significant targeting.

Key words

Copper bis(thiosemicarbazone), gold nanoparticles, smart-linked drug, targeted delivery, HeLa cell xenograft.

*Ashoka G. Samuelson *Department of Inorganic and Physical Chemistry, Indian Institute of Science, Bangalore- 560012, India* Email: ashoka@ipc.iisc.ernet.in
Kumaravel Somasundaram *Department of Microbiology and Cell Biology, Indian Institute of Science, Bangalore- 560012, India* Email: skumar@mcbl.iisc.ernet.in

Introduction

Cancer is one of the foremost causes for premature death.[1] Although chemotherapy increases the lifespan of cancer patients, the quality of life deteriorates significantly due to the non-specific cytotoxicity and inefficient delivery of anticancer drugs to the diseased tissue resulting in serious side effects.[2-4] A major challenge then, is to achieve selective delivery of the drug within cancer cells so that side effects are minimized.[5] In addition, if the drug is effective only in cancer cells and not in normal cells, one would have the magic bullet envisaged by Paul Ehrlich nearly a century ago.[6] Selective entry of the drugs to cancer cells requires them to be linked to a suitable targeting agent. Targeted drugs would then recognize cancer cells *via* receptors over expressed for the target on the surface of cancer cells and leave normal cells relatively unaffected.[7] Although conceptually simple, applying this paradigm to fight cancer is fraught with difficulties and so research in this area remains a major challenge.[8, 9]

In its simplest form, the targeting agent and the drug are both linked to a suitable delivery vehicle such as a simple polymer like polyethylene glycol, or to a more complex system like a dendrimer,[10] vesicle,[11] liposome,[12] nanoparticle,[13] or a nanotube.[14] Large delivery agents have an additional advantage in having many copies of the drug and the targeting agent on a single entity, increasing the probability of targeting cancer cells and killing them. If the large molecule is nanosized, they are also "passively targeted" as they leave the blood circulation system only in the vicinity of solid tumors due to the leaky vasculature characteristic of rapidly proliferating cancer cells in solid tumors.[15] Re-entry into the blood vessel is also less probable, leading to what is known as the Enhanced Permeation and Retention (EPR) effect.[16] Suitable decoration of the nanoparticle can also improve solubility, *in vivo* stability, prolonged blood circulation time and selective biodistribution.[17] For the drug to be effective, it has to be released from the delivery agent which, either requires the presence of a cleavable linkage or binding of the drug to the carrier *via* weak non-covalent interactions.[18, 19] This provides an opportunity to have another level of control in the release and activation of cytotoxic agents in side cancer cells. Smart release of the attached drugs from the nanocarrier can be triggered by cancer specific conditions such as higher levels of GSH in the cell, acidic pH or even by local application of heat or light on the affected tissue.[20-23] Nanomedicine has immense potential with wide ranging applications from simple therapy, to detection, diagnosis and theranostics.[24]

AuNPs are being extensively investigated for targeted drug delivery of drugs by tethering them to homing agents like antibodies, folic acid, biotin, suitable peptides, or monoclonal antibodies.[25-28] The synthesis, functionalization and loading of drugs is easier in the case of AuNPs in comparison to other nano particles. Studies on AuNPs have shown that capping them with polyethylene glycol improves their lifetime in the circulatory system and hence the bioavailability of their payload improves significantly at the desired site.[29, 30] AuNPs targeted in this fashion can home in on cancer cells and deliver their payload to the cells by receptor mediated endocytosis (active targeting) and these large nanoconjugates (less than 200 nm) exit only through the leaky blood vessels near the tumor tissue (passive targeting) which in turn improves the pharmacokinetics.[31-33]

Among the various metal complexes studied for anticancer activity, transition metal complexes, especially copper containing bis(thiosemicarbazone) ligands are extensively studied.[34, 35] Some of these complexes show cytotoxicity similar to cisplatin, the drug widely used in clinics.[36] Based on the mechanistic studies carried out on several copper(II) bis(thiosemicarbazone) complexes, particularly derived from glyoxal, it is generally believed that their cytotoxicity is a result of reactive oxygen species (ROS) they generate, whereas other complexes activate multiple pathways such as inhibition of DNA and RNA synthesis and disruption of ATP production resulting in apoptosis and growth inhibition.[37, 38] Although these complexes, like most copper(II) complexes, suffer from low water solubility and specificity, a few of them including CuATSM and amine terminated CuATSM (CuATSM-A) show selectivity towards hypoxic cells, again a characteristic feature of solid tumors, which results in accumulation of toxic copper in cancer cells.[39-41]

We hypothesized that conjugation of these molecules to a water soluble nanocarrier decorated with biotin as a targeting agent, and its delivery to the desired site by capitalizing on the EPR effect might improve their chance of being used as drugs.[42] Furthermore, if the link between the nano delivery agent and the copper complex is cleaved by GSH, the complex would be released inside cancer cells.[43] To this end we have synthesised a Cu(II) bis(thiosemicarbazone) complex, a close analog of CuATSM, by linking it to a PEG decorated gold nanoparticle through a redox active linker- a disulfide bond. We have examined its cytotoxicity against HeLa and HaCaT cells *in vitro* and its effectiveness in growth inhibition of a tumor expressed in nude mice using a

HeLa cell xenograft model. The biotin targeted vehicle was more effective in inhibiting the tumor growth *in vivo* than the simple gold nanoparticle.

Results and Discussion

Synthesis and characterization of a smart-linked cytotoxic agent: Copper(II) bis(thiosemicarbazone) complex (CuATSM-SS-COOH)

In order to make smart delivery of the copper bis(thiosemicarbazone) complex possible, a disulfide linker with a carboxylic acid group to link it to the delivery agent was attached to it (**Scheme 1).** The amine terminated biacetyl-bis(4-methyl-3-thiosemicarbazone) ligand, ATSM-A, was prepared following the literature procedure and the structure was confirmed by ^{1}H NMR spectroscopy and ESI-HRMS spectrometry.[44] ATSM-A was conjugated with 3,3´-dithiobis(propionic acid) in the presence of 1.1 equivalents of O-benzotriazole-N,N,N',N'-tetramethyl-uronium-hexafluoro-phosphate (HBTU) and N,N-diisopropylethylamine (DIPEA). ^{1}H NMR and ^{13}C NMR spectroscopy and ESI-HRMS confirmed the successful synthesis of the ligand, ATSM-SS-COOH (**Figure S1-S3**). Two singlets at 2.20 and 2.23 ppm in the ^{1}H NMR spectrum were assigned to the six methyl protons of the biacetyl unit, whereas a doublet at 3.01-3.03 ppm was due to the methyl group on the nitrogen split by the NH proton. Two multiplets at 2.57-2.65 ppm and 2.89-2.96 ppm correspond to the methylene protons of the disulfide linker. The ratios of the peaks assigned to ATSM-A to the disulphide linker corresponded to the formation of ATSM-SS-COOH. The corresponding copper complex, CuATSM-SS-COOH, was prepared by reaction of the ligand with copper acetate and was characterized by ESI-HRMS spectrometry and elemental analysis (**Figure S4** and **S5**).

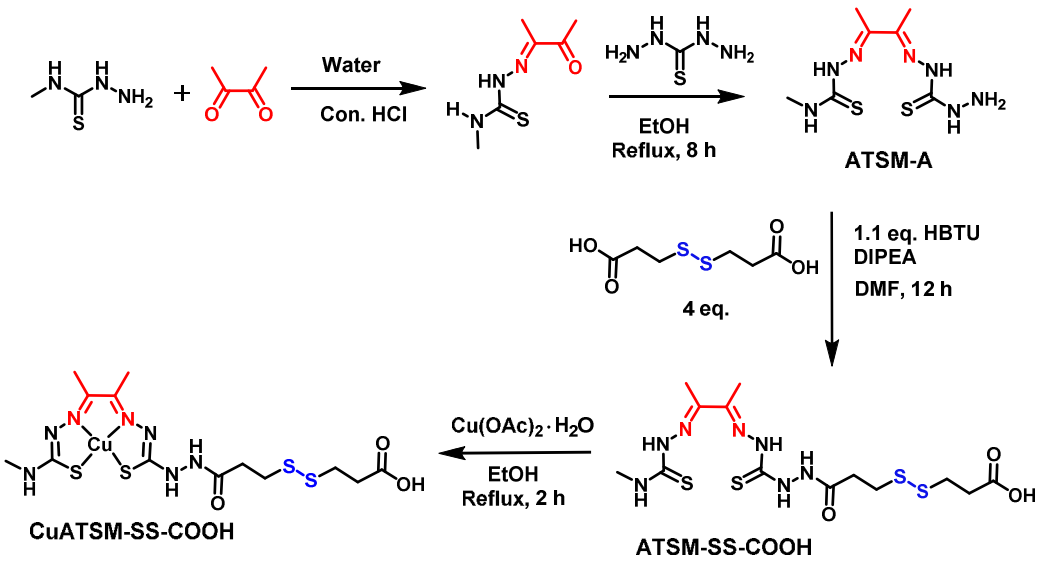

Scheme 1: Synthetic scheme for the preparation of CuATSM-SS-COOH.

Synthesis and characterization of lipoic acid functionalized polyethylene glycol

The use of lipoic acid, a cyclic disulphide, to anchor PEG to the gold nanoparticle has shown greater stability in the biological milieu compared to the use of mono-thiols.[45] Hence a capping agent, was prepared by reacting PEG-bis(amine) with N-hydroxysuccinimide activated lipoic acid (LA-NHS) in the presence of a weak base, $NaHCO_3$ following the literature procedure to give lipoic acid conjugated PEG (LA-PEG) (**Scheme 2**).[46, 47] The mono-functionalized PEG was purified by size exclusion chromatography (SEC) using lipophilic Sephadex LH-20 with methanol as eluent. Its structure was confirmed using ^{1}H NMR spectroscopy (**Figure S11**) prior to its use as the capping agent for stabilizing the gold nanoparticles.

Synthesis and characterization of PEGylated AuNP and nanoconjugates

Colloidal gold nanoparticles were prepared by the Turkevich-Frens method using trisodium citrate as the reducing agent in water,[48, 49] followed by ligand exchange with LA-PEG resulting in highly stabilized AuNPs (**Scheme 2**). AuNP-1 prepared in this fashion was purified by dialysis against Milli-Q water using a dialysis tube (MWCO: 12 kDa) and solid AuNP-1 was obtained after lyophilisation of the purified solution. A surface plasmon resonance band (SPR) at 526 nm (λ_{max}) confirmed the formation of PEGylated AuNPs (**Figure 1**). TEM images reveal aspherical AuNPs without any agglomeration of the nanoparticles (**Figure 2**). The core size of

nanoparticles was calculated by taking the average size of a large number of particles from TEM images. The histogram of the particle size shows a narrow distribution with an average diameter of 19.4 ± 1.9 nm**.** Further, the average height (17.7 ± 1.7 nm) of the nanoparticles in the AFM images is reasonably close to the size estimated from TEM measurements **(Figure 3)**. The stabilization of nanoparticles by the PEG linker was confirmed by ^{1}H NMR spectroscopy and further supported by FTIR spectroscopy by the presence of bands at 2880 cm^{-1} (-CH stretching), 1655 cm^{-1} (C=O stretching), 1541 cm^{-1} (N-H bending).[50] The extent of the surface functionalization by LA-PEG was estimated from thermogravimetric (TGA) analysis (**Figure S13**). Thermal decomposition pattern of AuNP-1 was similar to that of LA-PEG for which decomposition started at 300°C and ended at 420°C, with a weight loss of 89% suggesting a gold core accounting for the remaining 11% coated with LA-PEG. (**Table-S1**)**.**

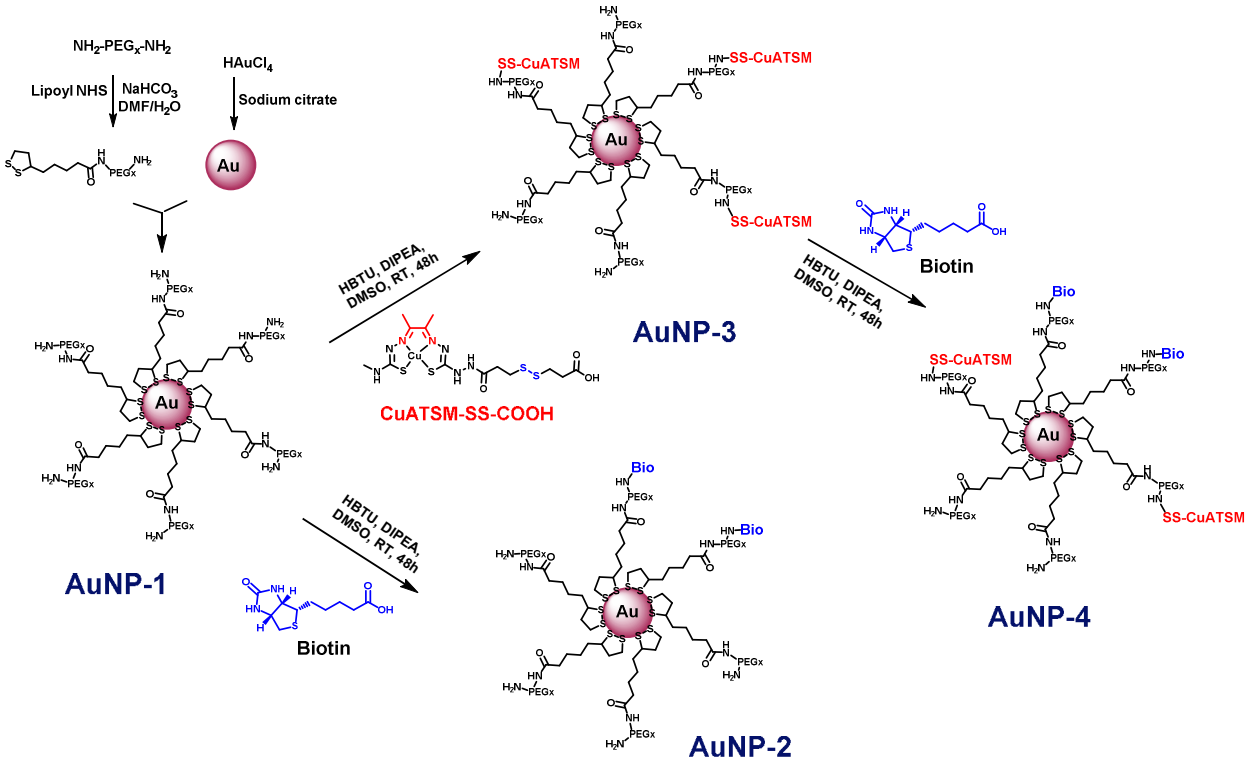

Scheme 2: Schematic illustration for the synthesis of PEG stabilized gold nanoparticles and nano-conjugates.

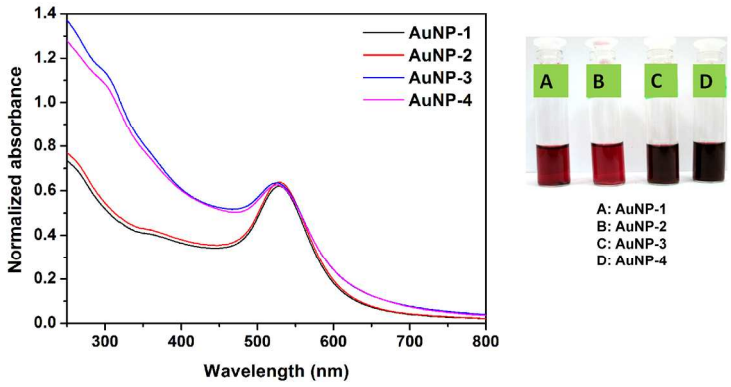

Figure 1: UV-visible spectra of PEG stabilized gold nanoparticles and nanoconjugates in Milli-Q water.

Synthesis and characterization of biotin containing nanoconjugates

Biotin was attached to AuNP-1 using the HBTU/DIPEA amide coupling protocol to link the carboxylic acid groups of biotin and the amine groups on the AuNP-1 surface thus creating AuNP-2. There was no shift in the SPR band of AuNP-2 after conjugation of biotin indicating stability of the nanoconjugate. Excess reagents were removed from AuNP-2 by extensive dialysis against Milli-Q water and dry AuNP-2 was obtained from the purified solution by freeze drying. Biotin conjugation on AuNP-2 was confirmed by the presence of two sets of doublet of doublets between 4.38-4.41 and 4.58-4.60 ppm in the ^{1}H NMR spectrum of the conjugate corresponding to two protons on the ring of biotin.[51] Particle size was measured from TEM and AFM images (**Figure 2** and **3, Table 1**) and the PEG content was estimated from TGA analysis (**Figure S13, Table S1**). The extent of biotin loading on the nanoparticles was estimated using the biochemical HABA assay to be 71.4 ± 3.3 nmol/mg of nanoconjugates present in AuNP-2 (**Table S2**).

Synthesis and characterization of drug and biotin containing nanoconjugates

The copper complex, CuATSM-SS-COOH, containing a carboxylic acid end group was conjugated to the amine group of AuNP-1 following the same amide coupling procedure leading to AuNP-3. To make the targeted nanocarrier, biotin was added to AuNP-3 using the same HBTU/DIPEA coupling agent resulting in AuNP-4 which was purified by the same techniques described earlier and the solid nanoconjugate was obtained by freeze drying. The average size of

AuNP-3, and AuNP-4, estimated from TEM and AFM images presented in the **Table 1**. These values suggest that there is no appreciable change in the size of the nanoconjugates after conjugation of the drug and/or biotin. More importantly, TEM and AFM images reveal there is no agglomeration or collapse of nanoconjugates which is also confirmed by no shift in the SPR band of AuNP-3 and AuNP-4 (**Figure 2** and **3, Table 1**). The hydrodynamic radius for the nanoconjugates were obtained from dynamic light scattering (DLS) measurements (**Table-1**) which showed no change in hydrodynamic radius after conjugation of biotin or CuATSM-SS-COOH to PEGylated AuNPs signifying the stability of the conjugates.

The drug loading was estimated from the copper content in the nanoconjugates by inductively coupled plasma mass spectrometry (ICP-MS) and found to be 1.11 ± 0.04 and 1.30 ± 0.20% in AuNP-3 and AuNP-4 respectively (**Table S3**). The amount of biotin, the targeting agent, attached to AuNP-4 was estimated using the HABA assay and found to be 25.1 ± 0.8 nmol/mg of nanoconjugates (**Table S2**). All the freeze dried nanoconjugates were stored at 4°C. [52]

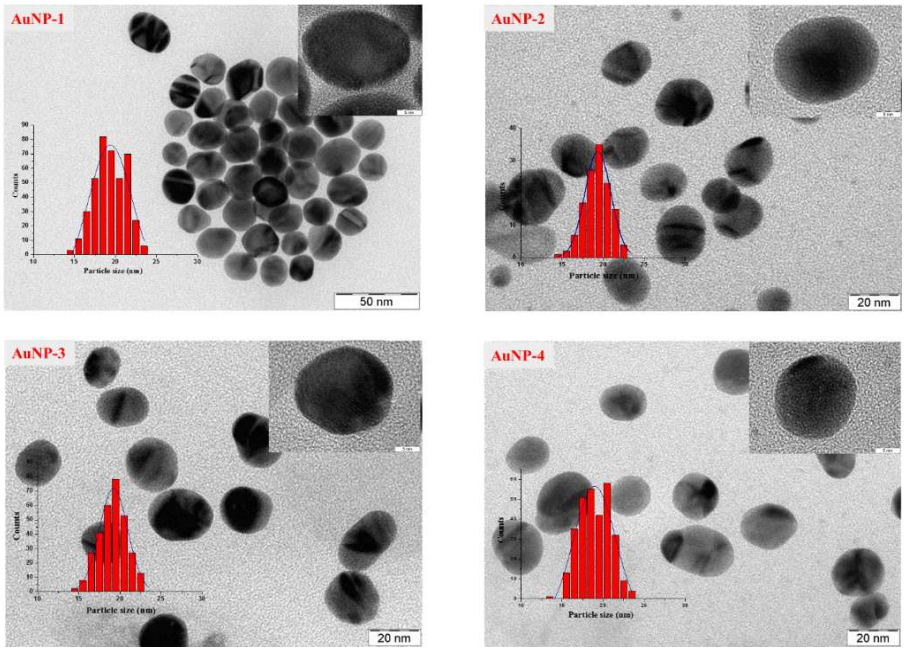

Figure 2: Transmission electron microscopy images and particle size distributions of AuNP-1 (top left), AuNP-2 (top right), AuNP-3 (bottom left), and AuNP-4 (bottom right). HRTEM is shown on the right-top of each image and the histogram (inset) shows the particle size distribution.

Table 1: Summary of the particle size of AuNPs from TEM, AFM and DLS measurements ± standard deviation (SD).

Nanoparticle	Size from TEM(nm)	Size from AFM(nm)	Hydrodynamic radius(nm)
AuNP-1	19.4 ± 1.9	17.7 ± 1.7	30.8 ± 1.0
AuNP-2	19.2 ± 1.9	19.2 ± 1.9	29.1 ± 1.8
AuNP-3	19.2 ± 1.6	18.7 ± 1.8	29.9 ± 1.6
AuNP-4	19.0 ± 1.8	19.5 ± 2.2	28.7 ± 1.8

Colloidal stability of nanoconjugates

Evaluation of colloidal stability of nanoconjugates under physiological conditions is essential before one can use nanoparticles in biomedical applications as they are exposed to different electrolyte and pH conditions on its journey from the point of administration to the tumor site. The pH in the blood stream is 7.3-7.5 whereas pH in endosomes (pH 5.0-6.5) and lysosomes (pH 4.5-5.0) are very low.[53] So, the nanoconjugate should be stable in a wide range of pH. As the SPR is very sensitive to aggregation, the stability of gold nanoparticles can be monitored by following the UV-visible profiles at different pH. No shift was observed in the SPR bands for AuNP-1 and AuNP-4 at different pH, moreover, there was no new peak appearing in the spectra (**Figure S15** and **S16**). Thus, it was concluded that the nanoconjugates used in the current study were stable in a wide range of pH and suitable for biological applications. AuNPs under investigation showed no discernible change in the intensity or position of the absorbance band at 526 nm at different concentrations of NaCl (**Figures S17 and S18**) ensuring their stability under different electrolyte concentrations.[54]

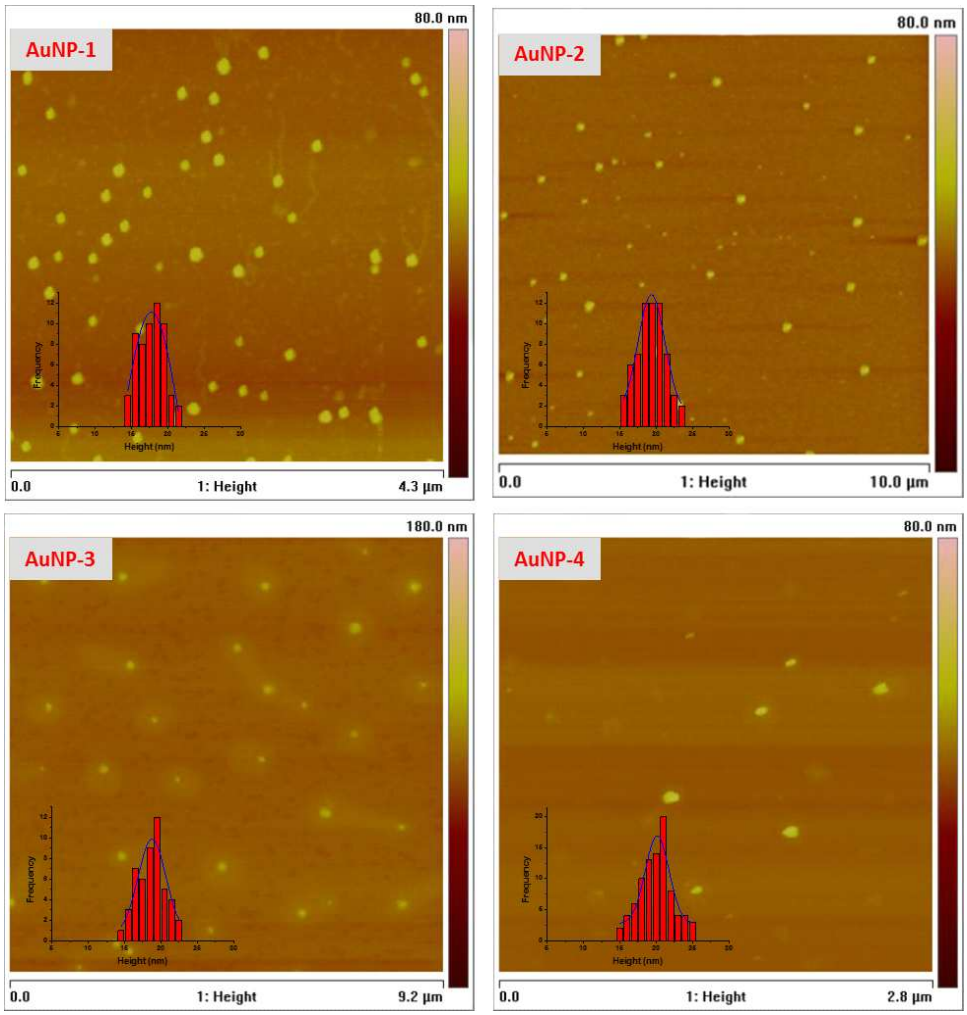

Figure 3: AFM images and height distribution of AuNP-1(top left), AuNP-2 (top right), AuNP-3 (bottom left), and AuNP-4 (bottom right).

GSH mediated drug release kinetics

Glutathione (GSH), an important redox active biomolecule reduces the disulfide bond.[55] The concentration of GSH in the extracellular medium is low, whereas within the cell it is relatively high.[56] Additionally, some tumor tissues have up to 7-fold higher concentration of GSH due to the highly reducing and hypoxic condition in them compared to normal tissues.[57, 58] The release kinetics of the drug from the nanoconjugates in presence of GSH was estimated to understand its activity. Cleavage of the disulfide bond caused by GSH at 5 mM concentration and release of the conjugated drug was followed by analysis of the copper content of dialyzed solutions at different

time points for 48h using ICP-MS (**Figure 4**). The release profile indicated a slow and partial release (about 60%) after 48h whereas in the absence of GSH as a trigger, there was less than 10% release of the conjugated drug in the same time period. This trend is in line with previous results where others have also observed slow and incomplete release of the conjugated drugs linked through a disulfide in the presence of GSH. Huo *et al.* reported 82% and 52% release of paclitaxel from a redox-sensitive polyethene glycol−paclitaxel prodrug over a period of 48h in the presence of 20mM and 10mM of GSH respectively.[59] The controlled and slow release of the drug could be advantageous to maintain an effective drug concentration in cancer cells which will increase the therapeutic efficacy of the drug.[60] The fact that *in vitro* release increases more than 80% with excess GSH suggests that the release is controlled by an equilibrium and would be controlled by the concentration of GSH in the cell being tested. Hence it is unlikely that inaccessibility of the S-S bond for cleavage is a reason for incomplete release.

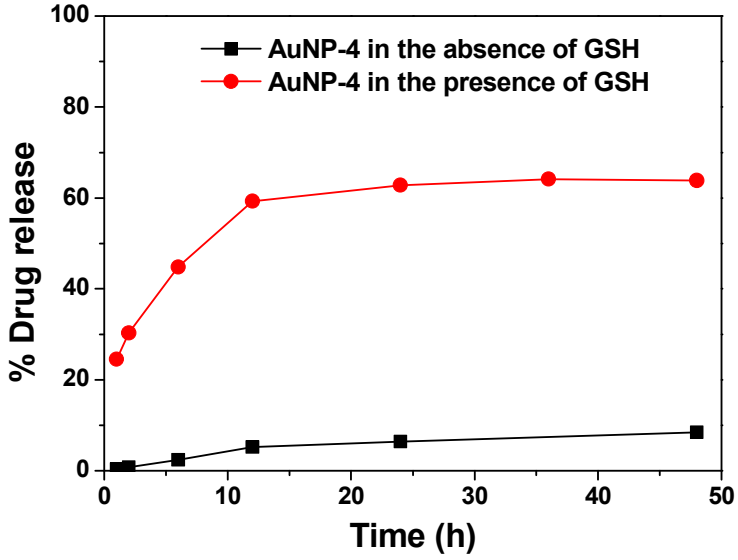

Figure 4: GSH triggered drug release profile of AuNP-4 in PBS solution at 37^0 C.

***In Vitro* Cytotoxicity:**

Copper(II) bis(thiosemicarbazone) complexes have been shown to be active against several cell lines [61-63] of which the cervical tumor cell line, HeLa is one of the most studied. It has been shown that Hela cells overexpress biotin-specific receptors.[64] Dong *et al.* have shown enhanced cellular uptake of the biotinylated gold nanoparticles by HeLa cells compared to A549 (lung cancer), MG63 (osteosarcoma) or NIH3T3 (normal fibroblast) cells.[65] The higher uptake of

biotinylated polyamidoamine (PAMAM) dendrimer with respect to the conjugate without biotin has been shown to be energy dependent.[66] So in the current study, the targeting efficacy of biotinylated AuNP carriers of the drug has been probed using the HeLa cell line. The unconjugated disulfide containing the copper complex, CuATSM-SS-COOH, showed very good cytotoxicity with $IC_{50} = 6.9 \pm 0.2$ μM which is the concentration required to kill 50% of the cells (**Figure 5a**). A model compound with disulfide linker between two bis(thiosemicarbazone) moiety, CuATSM-SS-CuATSM, was also checked for cytotoxicity and was found to have a similar activity, $IC_{50} = 7.2 \pm 0.8$ μM (**Figure 5a**). The nanoparticle, AuNP-1, and the biotinylated nanoparticle, AuNP-2 demonstrated no cytotoxicity up to 50 μg/ml in HeLa cells (**Figure S19**). Hence, AuNP-1 and AuNP-2 were considered safe for the delivery of the cytotoxic agents specifically to the tumor cells. Unlike AuNP-1 and AuNP-2, AuNP-3, a CuATSM-SS-COOH tethered AuNP-1, and AuNP-4, a biotinylated AuNP-3, were found to have IC_{50} values of 15.2 ± 0.3 μM and 17.7 ± 1.0 μM respectively in HeLa cells (**Figure 5a** and **Table 2**). The cell viability was also checked against non-tumorigenic immortalized keratinocyte cells (HaCaT) and the data is compared with the cytotoxicity values obtained with HeLa cells (Table 2). The IC_{50} of model copper complexes are significantly higher against HaCaT cells thus implying that the complexes are less cytotoxic to normal cells (**Figure 5b and Table 2**). In good correlation, AuNP-3 and AuNP-4, are also found to be less cytotoxic against HaCaT cells than against HeLa cells as well (**Figure 5b and Table 2**).

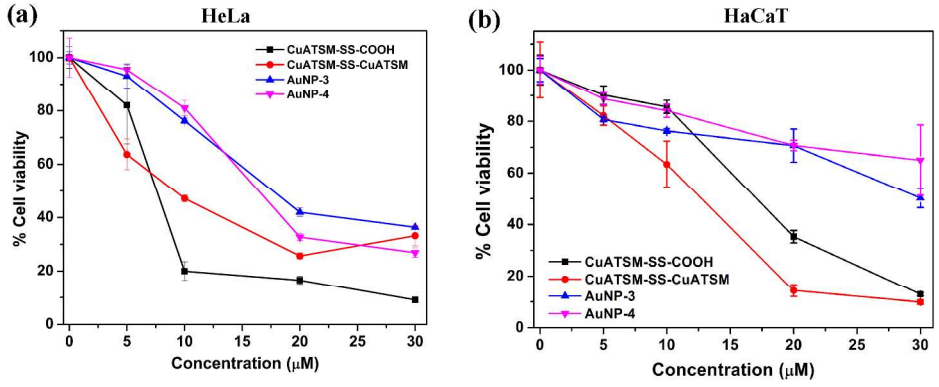

Figure 5: Cell viability of (a) HeLa cells and (b) HaCaT cells on treatment with CuATSM-SS-COOH, CuATSM-SS-CuATSM, AuNP-3 and AuNP-4 assessed by MTT assay at 48 h incubation. Data are presented as the mean of triplicate measurements ± SD.

Table 2: Summary of the cell viability of HeLa and HaCaT cells on treatment with CuATSM-SS-COOH, CuATSM-SS-CuATSM, AuNP-3 and AuNP-4.

Compound	IC_{50} (μM)	
	HeLa	HaCaT
CuATSM-SS-COOH	6.9 ± 0.2	19.6 ± 1.7
CuATSM-SS-CuATSM	7.2 ± 0.8	11.9 ± 1.1
AuNP-3	15.2 ± 0.3	30.0 ± 2.0
AuNP-4	17.7 ± 1.0	> 30

The reduced cytotoxicity observed for the drug nanoconjugate compared to the free drug is in keeping with observations made by others. The delivery of cisplatin through PEGylated PRINT hydrogel against A549, SKOV-3 (ovarian cancer) and MDA-MB-468 (breast cancer) showed less cytotoxicity compared to cisplatin due to slow and incomplete release of the drug which was approximately 60% after 72h.[67] Yu *et al.* demonstrated reduced activity of doxorubicin (DOX) on magnetic DOX-anchored nanogel (MDAN-gel) against HeLa cells and the result was attributed to the partial release of the drug from the nanoconjugate.[68] In this study also, the reduced activity of AuNP-3 and AuNP-4 compared to the parent drug could be ascribed to the slow and partial release of the active component. The expected increase in cytotoxicity of the biotinylated nanoconjugate was not observed *in vitro*, however, *in vivo* results proved more encouraging (*vide infra*). The reason for this apparent lack of targeting in the *in vitro* experiment is not obvious. However, the reduced cytotoxicity of the complexes and the nano-conjugates towards normal cells (HaCaT) could prove advantageous for *in vivo* applications.

Quantification of *in vitro* drug uptake by ICP-MS

For an anticancer agent to act, it has to first enter the cancer cell and activate pathways leading to cell death. So the activity or the cytotoxicity should be directly correlated to the amount of drug internalized by the cells. Drug internalization was estimated by ICP-MS by measuring copper content in the whole cell following a 6h incubation. Copper content nearly doubled from 0.67±

0.03 to 1.44 ± 0.33 in the case of AuNP-3 incubated cells. Biotin decorated AuNP-4 also showed a similar increase. Although the expected enhanced uptake with biotinylated AuNP-4 was not observed in HeLa cells, the similar drug uptake of AuNP-3 and AuNP-4 is consistent with the *in vitro* MTT assay result (**Figure 6**). As an excess of biotin was being used in the functionalization step, further increase in the extent of biotinylation of the gold nanoparticle was not possible with the current protocol. Decoration of the nanoparticle with more biotin is probably inhibited by the presence of copper bis(thiosemicarbazone) complex.

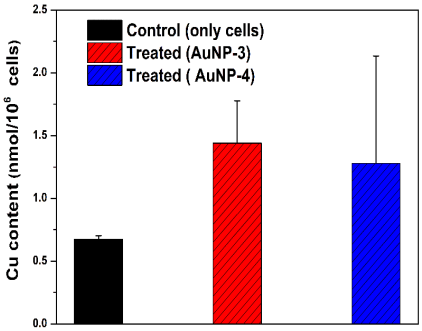

Figure 6: Drug uptake estimated from copper content estimated by ICP-MS in Hela cells 6h post treatment with AuNP-3 and AuNP-4.

Biotinylated gold nanoparticle, AuNP-4 is an efficient inhibitor of tumor growth

Biotin containing drug delivery systems have been shown to target tumor sites in animal models.[69-72] Biotin tagged polymeric nanoparticles encapsulated with paclitaxel demonstrated significant inhibition of tumor growth in a mouse model compared to the drug bearing nanoparticles without the biotin tag.[70] Biotin conjugated human serum albumin nanoparticles carrying methotrexate (MTX) was able to inhibit tumor growth of a breast tumor model in mice with enhanced therapeutic effect and reduced side effects compared to the non-targeted nanoparticle.[73] Hence, we decided to take up an *in vivo* study of AuNP-3 and AuNP-4. A solid tumor cervical xenograft model induced in nude mice with HeLa cells was used for this purpose and has been described in detail earlier.[74] Tumor volumes were compared in four groups of animals. The first group (Control) had saline treated mice whose tumors increased rapidly, the second group consisted of AuNP-2 treated mice which did not have significant inhibition compared with the control group (saline treated) as expected (Figure 7). In contrast, AuNP-3 treated mice (third group) showed 2.3-fold tumor growth inhibition at the end of 18 days.

Furthermore, AuNP-4 treated mice (fourth group) showed higher tumor growth inhibition than the third group with the reduction in tumor volume reaching a 3.8-fold compared with the AuNP-2 treated group. The percentage tumor growth was plotted for these four groups as a function of time (**Figure 7**). A two-way ANOVA test showed the comparisons to be very significant ($p < 0.001$). Although, *in vitro* studies showed that AuNP-3 and AuNP-4 exhibited similar activity with no enhancement from biotin conjugation (**Figure 5a**), *in vivo* tumor growth inhibitory effect of biotin conjugated nanoparticle (AuNP-4) was significantly better compared with AuNP-3 treated mice (**Figure 7** and **Figure S20**).

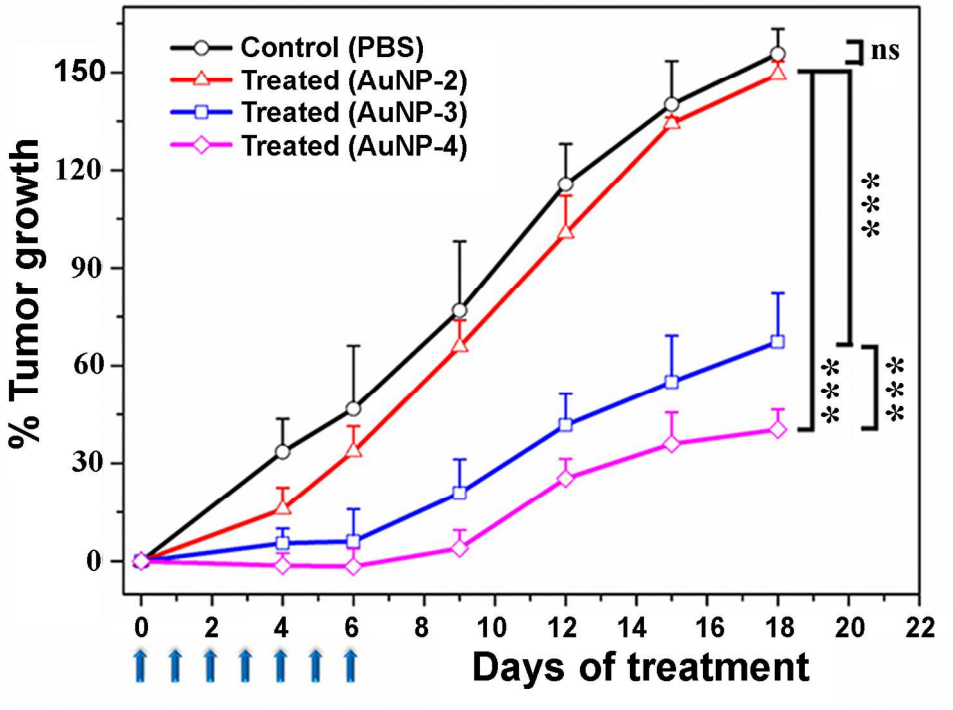

Figure 7: ***In vivo*** **anticancer activity of AuNPs in mice bearing HeLa xenografts. Mice received a dosage of 7.5 mg/kg/d nanoconjugates, AuNP-2, AuNP-3 and AuNP-4 and vehicle (PBS) daily for 7 days by ip injection. Arrows at the bottom of the figure indicates the treatment days. Tumor volumes were measured at regular intervals. Tumor volumes are expressed with ± standard error. Statistical analysis was made between different groups by 2-way ANOVA with the Bonferroni test for post hoc comparisons. ns refers to no significance, *** indicates $p < 0.001$.**

Mice in all the four groups had no systematic weight loss during the experiment suggesting absence of systematic toxicity of the targeted or non-targeted AuNPs (**Figure 8**).[75] Thus, drug conjugation to gold nanoparticles increased drug efficacy without increasing toxicity.

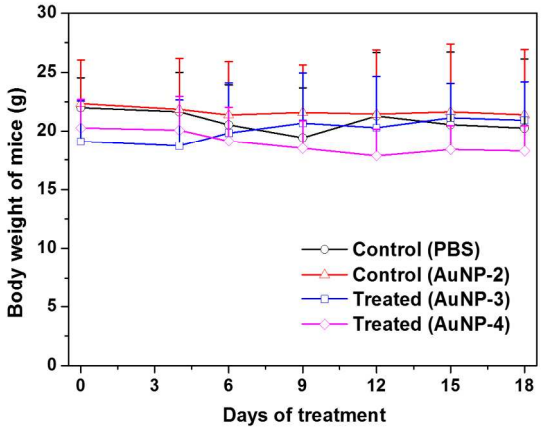

Figure 8: Plot of body weight of treated mice during treatment. Data are presented as the mean ± SD.

Conclusions

We have demonstrated the first smart delivery of a copper bis(thiosemicarbazone) complex, CuATSM-SS-COOH, using AuNPs stabilized by PEGylation. *In vivo* targeted delivery of these gold nanoparticles by biotin decoration has also been established. Unlike the copper complex, Cu-ATSM and its close analogs, the AuNP conjugates have very good aqueous solubility and stability in a wide range of pH and salt concentrations. Substantial release of the cytotoxic agent with cellular reducing agents, such as GSH could be achieved, and demonstrated *ex-vivo.* Although, this smart linking reduced the cytotoxicity of AuNP-3 and AuNP-4 relative to the parent copper complex, *in vivo* studies demonstrated the effectiveness of these nanoparticle carriers as suitable delivery vehicles as they exhibited efficient reduction of tumor volume without significant loss in body weight. Moreover, we also found that the biotin conjugated gold nanoparticle, AuNP-4, was more efficient in inhibiting the tumor growth compared to the gold nanoparticle without biotin, AuNP-3. This smart linking strategy can be extended to other cytotoxic complexes that suffer from non-specificity, low aqueous solubility and toxicity. Our current efforts are directed towards finding better complexes to link and improving biotin loading.

Experimental Section

Materials and Methods

N-hydroxy succinimide, polyethylene glycol (MW 3000), (±)-α-lipoic acid, Sephadex LH-20, 3-mercaptopropionic acid, and dialysis tubing (12 kDa MWCO) were purchased from Sigma Aldrich. Dialysis tubing (3.5 kDa MWCO) was purchased from ThermoFischer Scientific. $HAuCl_4$, citrate were obtained from SRL chemicals (India). *N*, *N*'-Dicyclohexylcarbidoimide (DCC) was purchased from Spectrochem Pvt. Ltd. (India). O-Benzotriazole-N,N,N',N'-tetramethyl-uronium-hexafluoro-phosphate (HBTU), N,N-diisopropylethylamine (DIPEA) were obtained from Avra Synthesis Pvt. Ltd. (India). Water was purified using Biocel Milli-Q water purification system (18.2 MΩ cm^{-1}) and used for all experiments. All the solvents were dried and distilled prior to use, following standard procedures. Standards for ICP-MS analysis were purchased from Fluka Analytical.

^{1}H and ^{13}C NMR spectra were recorded in Bruker AMX 400 spectrometer (operating at 400 and 100 MHz respectively). UV-vis spectra were recorded using Perkin Elmer Lambda 35 UV-visible spectrometer. IR spectra in KBr phase were obtained from Perkin Elmer Spectrum One FT-IR spectrometer. TEM images were obtained from samples placed on a carbon coated copper grid using a JEOL 2100F instrument operated with an accelerating voltage of 200 kV. AFM images were acquired on Multimode Scanning Probe Microscope using a NanoScope IV A controller using the tapping mode on the cleaved mica surface. TGA analysis of the samples were done on a NETZSCH TG 209 F1 thermogravimetric analyzer. The copper content of the nano-conjugates was estimated using a Thermo Scientific XSeries 2 ICP-MS. Mass spectra were recorded using Agilent 6538 ultra-high definition (UHD) accurate-mass Q-TOF (LC-HRMS) instrument. Brookhaven ZetaPALS instrument was used to determine hydrodynamic radius of the nanoconjugates. Copper content in nanoconjugates and in cells was estimated using a Thermo Scientific XSeries 2 inductively coupled plasma mass spectroscopy (ICP-MS).

Synthesis of ATSM-SS-COOH:

Bis(thiosemicarbazone) ligand with a disulfide linker was synthesized as follows. Initially, the ATSM-A was prepared according to the previously reported procedures (**Scheme 1)**.[44, 76] A solution of 3,3'-dithiobis(propionic acid) and HBTU in dry N,N-dimethyl formamide (DMF) was

stirred for 1h at 0°C in an ice-bath. After 1h, diacetyl-2-(4-N-methyl-3-thiosemicarbazone)-3-(4-N-amino-3-thiosemicarbazone) (ATSM-A) dissolved in dry DMF was added dropwise to the above mentioned ice-cold solution over a period of 15 min. Next, N,N-diisopropylethyl amine (DIPEA) was added to the reaction mixture. The resulting reaction mixture was then brought to room temperature and stirred for 24h. The reaction mixture was concentrated under vacuum at 65°C and subsequently added to a large excess of water which resulted in precipitation of a yellow solid. The precipitate was washed with copious amounts of water and dried in *vacuo*. Yield – 75%. ^{1}H NMR (400 MHz; DMSO-d_6): δ 2.20 (3H, s, CH_3), δ 2.23 (3H, s, CH_3), δ 2.57-2.65 (4H, m, CH_2-C=O), δ 2.89-2.96 (4H, m, CH_2-S), δ 3.01-3.03 (3H, d, N-CH_3), δ 8.40-8.41 (1H, d, NH), δ 8.40-8.41 (1H, d, NH), δ 9.98 (1H, s, NH), δ 10.16 (1H, s, NH), δ 10.25 (1H, s, NH), δ 10.61 (1H, s, NH), δ 12.34 (1H, s, COOH). ^{13}C NMR (100 MHz; DMSO-d_6): δ 12.5, δ 12.7 (CH_3), δ 32.1 (NCH_3), δ 34.0, δ 34.2, δ 34.3, δ 34.6 (CH_2), δ 148.7, δ 150.6 (C=N), δ 170.0 (COOH), δ 173.6 (C=O), δ 179.4, δ 180.1(C=S), ESI-HRMS calculated $[M\text{-}H^+]^-$: m/z – 452.0667, found m/z – 452.0716 (100%). Elemental analysis (%): calculated for $C_{13}H_{23}N_7O_3S_4.H_2O$: C – 33.1, H – 5.3, N – 20.8, S – 27.2, found ($C_{13}H_{23}N_7O_3S_4.H_2O$): C – 32.2, H – 5.5, N – 20.7, S – 26.8.

Synthesis of CuATSM-SS-COOH:

ATSM-SS-COOH (0.20 g, 0.44 mmol) was suspended in dry ethanol (10 mL) and copper acetate (0.09 g, 0.45 mmol) was added to the above mixture. The reaction mixture was refluxed for 6h at 80°C. The product was filtered and washed thoroughly with ethanol and dried *in vacuo*. Yield – 90%. ESI-HRMS calculated $[M\text{-}H^+]^-$: m/z – 512.9812, found m/z – 512.9817(100%), calculated $[M+H^+]^+$: m/z – 514.9957, found m/z – 514.9934(100%). IR data (cm^{-1}): 3365 (m, COOH), 3245 (m, NH), 2925 (m), 1670 (m, C=O), 1507 (s, C=N), 1395 (vs, amide), 1225 (vs, thioamide), 832 (w, C=S). UV−visible in DMSO [λ_{max}, nm (ε, M^{-1} cm^{-1})]: 312 (21750) and 475 (7320). Elemental analysis (%): calculated for $CuC_{13}H_{21}N_7O_3S_4$: C – 30.3, H – 4.1, N – 19.0, S – 24.9, found ($CuC_{13}H_{21}N_7O_3S_4$): C – 29.9, H – 4.1, N – 18.9, S – 24.6.

Synthesis of ATSM–SS–ATSM:

HBTU (0.50 g, 1.3 mmol) in DMF (3 mL) was added to DMF (3 mL) solution of 3,3′-dithiobis(propionic acid) (0.13 g, 0.62 mmol) and stirred for 1 h at 0 ˚C. In another flask,

ATSM/A (0.3 g, 1.2 mmol) was dissolved in DMF (10 mL). The ATSM/A solution was added slowly to the activated 3,3′-dithiobis(propionic acid) over a period of 15 min and then DIPEA (0.2 g, 1.6 mmol) was added. The resulting mixture was stirred for 6 h at room temperature under nitrogen. The reaction mixture was concentrated to about 2 mL by applying vacuum at 65 ˚C and the product precipitated out by the addition of water. The precipitate formed was washed with adequate amount of water to obtain ATSM–SS–ATSM as a brownish-yellow solid. Yield: 75% (0.3 g). ^{1}H NMR (400 MHz; DMSO-d_6): δ 2.20 (6H, s, C*H*$_3$), δ 2.23 (6H, s, C*H*$_3$), δ 2.59-2.63 (4H, t, C*H*$_2$ –C=O), δ 2.95-2.99 (4H, t, C*H*$_2$ –S), δ 3.02-3.03 (3H, d, C*H*$_3$), δ 8.39-8.40 (1H, q, N*H*-CH$_3$), δ 9.98 (1H, s, NH-C=O), δ 10.17 (1H, s, N*H*), δ 10.22 (1H, s, N*H*), δ 10.60 (1H, s, N*H*). ^{13}C NMR (100 MHz; DMSO-d_6): δ 12.6 (CH$_3$), δ 12.8 (CH$_3$), δ 32.1 (CH$_3$N), δ 34.2 (CH$_2$), δ 148.8, δ 150.6 (C=N), δ 170.1 (C=O), δ 179.4 δ 180.1 (C=S). ESI-HRMS calculated $[M+H^+]^+$: m/z – 697.1543, found m/z – 697.1553.

Synthesis of CuATSM–SS–CuATSM:

To a suspension of ATSM–SS–ATSM (0.12 g, 0.17 mmol) in ethanol (10 mL), copper acetate (0.069 g, 0.34 mmol) was added and refluxed for 4 h. The solution was cooled to room temperature and filtered, the precipitate washed with ethanol and dried *in vacuo* to give CuATSM–SS–CuATSM as a dark-brown solid (0.12 g). Yield: 86%. ESI-HRMS calculated $[M+H^+]^+$: m/z – 820.9801, found m/z – 820.9836. IR data (cm^{-1}): 3164 (m, NH), 1679 (m, C=O), 1484 (vs, C=N), 1224 (s, thioamide), 828 (w, C=S). UV−visible in DMF [λ_{max}, nm (ε, M^{-1} cm^{-1})]: 312 (31 200) and 480 (10300). Elemental analysis (%): calculated for $Cu_2C_{20}H_{32}N_{14}O_2S_6.2H_2O$: C – 26.9, H – 4.5, N – 21.9, S – 21.5, found ($Cu_2C_{20}H_{32}N_{14}O_2S_6.2H_2O$): C – 25.9, H – 3.7, N – 19.4, S – 20.4.

Synthesis of LA-NHS:

A solution of N-hydrosuccinamide (NHS) (0.40 g, 4.31 mmol) and *N*,*N*'-Dicyclohexylcarbidoimide (DCC) (1.5 g, 4.3 mmol) in dry DCM (60 mL) and DMF (2ml) was cooled to 0^{o} C in an ice bath. To this, (±)-α-lipoic acid (0.80 g, 3.9 mmol) in dry DCM (60 mL) was added. The reaction mixture was warmed up to room temperature and stirred for 48h in the dark. After 48h, the precipitated dicyclohexylurea (DCU) was filtered off and the solvent was evaporated under reduced pressure. Isopropanol was added to dissolve the crude product and

scratching the walls of the beaker resulted in the formation of a pale yellow solid which was filtered and washed with hexane. The product was air dried. Yield (0.64g, 55.0%). ^{1}H NMR (400 MHz, $CDCl_3$): 1.51-1.60 (2H, m, -$CHCH_2$), 1.69-1.81 (4H, m, -$COCH_2$), 1.88-1.96 (1H, m, -CH), 2.43-2.51 (1H, m, -CH), 2.61-2.64 (2H, t, -CH_2), 2.83-2.84 (4H, d, -NCH_2), 3.10-3.19 (2H, m, -SCH_2), 3.54-3.61 (1H, q, -SCH).

Synthesis of LA-PEG-NH_2:

Diamino-polyethylene glycol (PEG, MW 3000) was synthesized following the literature procedure.[77, 78] The capping agent, LA-PEG-NH_2, was prepared and purified in the following way. To a solution of diamine-PEG (8.05 g, 2.68 mmol) and sodium hydrogencarbonate (0.23 g, 2.70 mmol) in DMF/water (10 mL/10 mL) at 0°C, a solution of LA-NHS (0.49 g, 1.60 mmol) in DMF (3mL) was added dropwise. The solution was then brought to room temperature and stirred for 24h at RT. The product was extracted with $CHCl_3$ (3x50 mL). The organic fraction was washed with water (3x30 mL) and dried over anhydrous Na_2SO_4. The crude product was obtained by evaporation of the solvent and was purified by passing through a Sephadex (LH-20) column using methanol as eluent. Yield (3.8 g, 45 %). ^{1}H NMR (400 MHz, $CDCl_3$): 1.41-1.47 (m, -$COCH_2$-, 2H), 1.62-1.69 (m, -CH_2, 4H), 1.86-1.97 (m, -SCH_2CH_2, 1H), 2.15-2.19 (t, -CH_2-CONH-, 2H), 2.42-2.49 (m, -SCH_2CH_2, 1H), 2.89-2.92 (t, NH_2-CH_2, 2H), 3.43-3.80 (m, -$O(CH_2)_2$, 264H).

Synthesis of AuNP-1:

$HAuCl_4$ 0.03% in 400 mL of Milli-Q water was heated to boiling with vigorous stirring and a preheated (60°C) solution of trisodium citrate (0.18 g in 18 ml of Milli-Q water) was added. Within a few minutes a gradual color change from yellow to pink red was observed. The mixture was kept for another 15 min at the same temperature and then allowed to cool to room temperature naturally. LA-PEG-NH_2 (1.68 g) dissolved in 4 mL of Milli-Q water was added to the above colloidal solution and stirred overnight at RT. The LA-PEG-NH2 stabilized nanoparticle solution was concentrated and dialyzed (12 kDa MWCO) against Milli-Q water for 48h. Yield (0.50 g). ^{1}H NMR (400 MHz, D_2O): 1.17-1.21 (t, -CH_2, 2H), 1.35-1.47 (m, -$COCH_2CH_2$, 4H), 1.97-2.04 (m, -CH_2CH-, 1H), 2.25-2.29 (t, -CH_2CH_2, 2H), 2.44-2.51 (m, -

CH_2CH, 1H), 2.92 (br, NH_2-CH_2, 2H), 3.20-3.25 (m, -SCH_2, 2H), 3.39-3.89 (m, -$O(CH_2)_2$, 264H).

Synthesis of AuNP-2:

Biotin (1.9 mg, 7.8 μmol) dissolved in DMF (3 mL) was added dropwise at 0°C to a solution of HBTU (2.9 mg, 7.6 μmol) in DMF (2 mL). The solution was allowed to stir at room temperature for 1h. AuNP-1 (90 mg) in DMF (3 mL) was added drop wise to the solution at 0°C. After the addition, the mixture was allowed to stir for 15 min. To this DIPEA (7 mg, 0.05 mmol) was added and stirred overnight at room temperature. The reaction mixture was then dialyzed (12 kDa MWCO) against Milli-Q water for 48h (water changed every 6h), and finally lyophilized to get solid nanoparticles of AuNP-2. Yield - 65 mg.

Synthesis of AuNP-3:

CuATSM-SS-COOH (20 mg, 39.0 μmol) dissolved in DMF (3 mL) was added drop wise at 0°C to a solution of HBTU (16 mg, 42.2 μmol) in DMF (2 mL). The solution was allowed to stir at room temperature for 1h. AuNP-1 (235 mg) in DMF (3 ml) was added drop wise to the solution at 0°C. After the addition, the mixture was allowed to stir for 15 min. To this DIPEA (37 mg, 0.285 mmol) was added and stirred overnight at room temperature. The reaction mixture was then dialyzed (12 kDa MWCO) against Milli-Q water for 48h (water changed every 6h), and finally lyophilized to get solid nanoparticles. Yield - 180 mg.

Synthesis of AuNP-4:

Biotin was conjugated to AuNP-3 following the same procedure as that described for preparation of AuNP-2. To a solution of HBTU (3.8 mg, 10.0 μmol) in DMF (2 mL), biotin (2.4 mg, 9.8 μmol) in DMF (3 mL) was added drop wise at 0°C. The solution was allowed to stir at room temperature for 1h. AuNP-3 (115 mg) in DMF (3 mL) was added drop wise to the solution at 0°C. After the addition, the mixture was allowed to stir for 15 min. To this DIPEA (15 mg, 0.115 mmol) was added and stirred overnight at room temperature. Yield - 75 mg.

TEM and AFM characterization:

TEM samples were prepared by dissolving solid AuNPs in HPLC grade methanol (~ 0.5 mg/ml) and drop coating on 400 mesh carbon coated copper grid. For AFM, solutions of the samples in HPLC grade methanol were spin coated at 2000 RPM for 1 min on a cleaved mica surface and dried under vacuum.

GSH triggered release of copper complex:

AuNP-4 (5 mg) in 1mL PBS buffer (pH 7.4) was suspended in the dialysis tube (3.5 kDa MWCO). To this solution, GSH (3 mg, 9.77 μmol) in 1 ml PBS buffer (pH 7.4) was added. The dialysis tube was then immersed in a beaker having 160 mL of PBS buffer at 37°C for 48 h. A control experiment was also carried without GSH. In both the cases, at time intervals 0.5 h, 1 h, 2 h, 6 h, 12 h, 24 h, 32 h and 48 h; 2 ml of the outer solution was taken out and 2 ml of fresh PBS buffer (pH 7.4) was added to maintain the same volume. The copper content of the collected samples at different time intervals was estimated by ICP-MS analysis and the % of drug released plotted as a function of time.

Copper estimation by ICP- MS:

Three sets of HeLa cells (~10 million cells each) were treated with 25 μM of AuNP-3, AuNP-4 and one set of cells without any treatment were kept for 6 h at 37°C in a humidified 5% CO_2 incubator. After 6h, the media was removed to exclude unabsorbed nanoconjugates and the cells were washed with 5 ml of PBS, trypsinised, and collected in 5 ml of PBS. The scraped cells were spun down, by centrifugation at 2000 RPM for 5 min. The supernatant was discarded and the cells were once again washed with PBS. The cell pellet so obtained was suspended again and the number of cells were counted. Cells were lysed in 1M NaOH (1 mL) and diluted with 2% (v/v) HNO_3 (9 mL) for determining whole cell copper content. The instrument was calibrated using standard solutions containing 10, 50, 100, and 500 ppb copper.

Biotin estimation by HABA assay:

The degree of biotinylation in the biotinylated AuNPs was determined by HABA assay.[79] Briefly, the avidin/HABA reagent was prepared according to the manufacturer's instructions by adding 10 ml of Milli-Q water to the orange colored solid. The final solution contains 0.3 mM HABA, 0.45 mg/mL avidin, 0.3 M NaCl, 0.01 M HEPES, 0.01 M $MgCl_2$, 0.02% NaN_3 (as a

preservative). To a 1 mL cuvette 900 μL of HABA/Avidin solution was added. This was followed by 100 μL of biotin or, biotinylated AuNPs dissolved in PBS to make the final volume of 1 mL. As a control, 100 μL of PBS was added to the reference. For colored AuNPs samples, a separate blank was made with 900 μL water and 100 μL of conjugate. The absorbance was measured at 500 nm using a Perkin Elmer Lambda 35 UV-visible spectrometer. The calculations were done using the equation: $\Delta A_{500} = 0.9(A^{HABA/Avidin}) + A^{sample\ blank} - A^{HABA/Avidin + sample})$, 0.9 = dilution factor and μmole biotin/ml = $(\Delta A_{500}/34)\times 10$ where 34 = mM extinction coefficient at 500 nm and 10 = dilution factor. All measurements were done in triplicate.

***In vitro* cytotoxicity analysis by MTT assay:**

The MTT assay was carried out to measure cell viability as described earlier.[33] Two thousand cells in 100 μL of growth media (DMEM) were seeded in a 96-well plate and kept in CO_2 incubator. After 24 h, 100 μL of various concentrations of copper bis-(thiosemicarbazone) and nanoconjugate solutions were added and incubated for 48 h at 37°C in a CO_2 incubator. At the 45th hour after incubation, MTT (20 μL of 5 mg/ml) was added to the wells. After removing the media, the formazan crystals formed were dissolved in 200 μL of DMSO, and the absorbance was measured at 570 nm in a microplate reader (Molecular Devices, Spectramax M5e). The cytotoxic effects of complexes and conjugates were quantified by calculating the drug concentration inhibiting tumor cell growth by 50% (IC_{50}).

***In vivo* xenograft model:**

The anticancer activity of nanoconjugates was examined in a cervical xenograft model using HeLa cells as previously described.[64] Briefly, 10 million viable HeLa cells in 100 μL PBS were injected subcutaneously into the right posterior flank of each female nude mouse aged 4−5 weeks. After the tumor size reached approximately 200 mm^3, mice were divided into four groups with four animals in the first two groups (PBS treated and AuNP-2 treated) and five animals in the other two groups (AuNP-3 and AuNP-4 treated). The nanoconjugate (7.5 mg/kg body weight) dissolved in PBS was injected intraperitoneally (ip), and the control group was treated with an equal volume of the vehicle for seven consecutive days. The tumor volumes were measured at regular intervals. The tumor volume (T_v) was calculated using the formula: $\pi/6 \times$ (larger diameter) × (smaller diameter)^2. The tumor volume and mice body weight was monitored

for 18 days. The tumor growth was estimated using the formula: % tumor growth= $[(V_n-V_0)/V_n]\times100$, where V_n is tumor volume on n^{th} day of treatment and V_0 is the tumor volume on the first day of treatment. Tumor volume was measured using Vernier Calipers. Statistical analysis of the tumor volumes was made between different groups by 2-way ANOVA with the Bonferroni test for post hoc comparisons using GraphPad Prism 5 software. All experiments used in our animal studies were approved by the ethics committee of Indian Institute of Science for animal care and usage.

Author Information

Corresponding Author Phone: (+91) 80-2293-2973. Fax: (+91) 80-2360-2697. E-mail: skumar@mcbl.iisc.ernet.in (K.S.). Phone: (+91) 80-2293-2663. Fax: (+91) 80-2360-1552. E-mail: ashoka@ipc.iisc.ernet.in (A.G.S.).

Notes: The authors declare no competing financial interest.

Acknowledgement

A.K.P gratefully acknowledges Indian Institute of Science for a Senior Research Fellowship. K.S. and A.G.S. thank the Department of Science and Technology (New Delhi) and Department of Biotechnology (New Delhi) for the award of a research grant. K.S. is a J. C. Bose fellow (DST). We thank the Central Animal Facility, Indian Institute of Science (IISc), for providing the nude mice.

Supporting Information: Characterization data (NMR, ESI-MS, IR, TGA, and powder XRD spectra), AuNP stability study by UV-vis, data for estimation of biotin, ICP-MS data, images of tumor bearing mice. This material is available free of charge via the Internet at http://pubs.acs.org.

References:

(1) Siegel, R. L., Miller, K. D., and Jemal, A. (2015) Cancer statistics, 2015. *CA Cancer J. Clin. 65*, 5-29.
(2) Lima-Tenorio, M. K., Pineda, E. A., Ahmad, N. M., Fessi, H., and Elaissari, A. (2015) Magnetic nanoparticles: In vivo cancer diagnosis and therapy. *Int. J. Pharm. 493*, 313-27.
(3) Davis, M. E., Chen, Z. G., and Shin, D. M. (2008) Nanoparticle therapeutics: An emerging treatment modality for cancer. *Nat. Rev. Drug Discov. 7*, 771-82.

(4) Lim, E. K., Jang, E., Lee, K., Haam, S., and Huh, Y. M. (2013) Delivery of cancer therapeutics using nanotechnology. *Pharmaceutics 5*, 294-317.
(5) Patra, C. R., Bhattacharya, R., Wang, E., Katarya, A., Lau, J. S., Dutta, S., Muders, M., Wang, S., Buhrow, S. A., Safgren, S. L., et al. (2008) Targeted delivery of gemcitabine to pancreatic adenocarcinoma using cetuximab as a targeting agent. *Cancer Res. 68*, 1970-8.
(6) Strebhardt, K., and Ullrich, A. (2008) Paul ehrlich's magic bullet concept: 100 years of progress. *Nat. Rev. Cancer 8*, 473-480.
(7) Kumar, A., Zhang, X., and Liang, X. J. (2013) Gold nanoparticles: Emerging paradigm for targeted drug delivery system. *Biotechnol. Adv. 31*, 593-606.
(8) Muro, S. (2012) Challenges in design and characterization of ligand-targeted drug delivery systems. *J. Control Release 164*, 125-137.
(9) Howard, M., Zern, B. J., Anselmo, A. C., Shuvaev, V. V., Mitragotri, S., and Muzykantov, V. (2014) Vascular targeting of nanocarriers: Perplexing aspects of the seemingly straightforward paradigm. *ACS Nano 8*, 4100-4132.
(10) Mintzer, M. A., and Grinstaff, M. W. (2011) Biomedical applications of dendrimers: A tutorial. *Chem. Soc. Rev. 40*, 173-90.
(11) Johnson, R. P., Uthaman, S., John, J. V., Lee, H. R., Lee, S. J., Park, H., Park, I. K., Suh, H., and Kim, I. (2015) Poly(pega)-b-poly(l-lysine)-b-poly(l-histidine) hybrid vesicles for tumoral ph-triggered intracellular delivery of doxorubicin hydrochloride. *ACS Appl. Mater. Interfaces 7*, 21770-9.
(12) Al-Jamal, W. T., and Kostarelos, K. (2011) Liposomes: From a clinically established drug delivery system to a nanoparticle platform for theranostic nanomedicine. *Acc. Chem. Res. 44*, 1094-1104.
(13) Xu, P., Van Kirk, E. A., Zhan, Y., Murdoch, W. J., Radosz, M., and Shen, Y. (2007) Targeted charge-reversal nanoparticles for nuclear drug delivery. *Angew. Chem. Int. Ed. 46*, 4999-5002.
(14) Bianco, A., Kostarelos, K., Partidos, C. D., and Prato, M. (2005) Biomedical applications of functionalised carbon nanotubes. *Chem. Commun. (Camb.)*, 571-7.
(15) Kobayashi, H., Turkbey, B., Watanabe, R., and Choyke, P. L. (2014) Cancer drug delivery: Considerations in the rational design of nanosized bioconjugates. *Bioconjug. Chem. 25*, 2093-100.
(16) Prakash, S., Malhotra, M., Shao, W., Tomaro-Duchesneau, C., and Abbasi, S. (2011) Polymeric nanohybrids and functionalized carbon nanotubes as drug delivery carriers for cancer therapy. *Adv. Drug Deliv. Rev. 63*, 1340-51.
(17) Kunjachan, S., Ehling, J., Storm, G., Kiessling, F., and Lammers, T. (2015) Noninvasive imaging of nanomedicines and nanotheranostics: Principles, progress, and prospects. *Chem. Rev. 115*, 10907-37.
(18) Böhme, D., and Beck-Sickinger, A. G. (2015) Drug delivery and release systems for targeted tumor therapy. *J. Pept. Sci. 21*, 186-200.
(19) Lim, E.-K., Jang, E., Lee, K., Haam, S., and Huh, Y.-M. (2013) Delivery of cancer therapeutics using nanotechnology. *Pharmaceutics 5*.
(20) Green, R. M., Graham, M., O'Donovan, M. R., Chipman, J. K., and Hodges, N. J. (2006) Subcellular compartmentalization of glutathione: Correlations with parameters of oxidative stress related to genotoxicity. *Mutagenesis 21*, 383-90.
(21) Li, Y., Xiao, W., Xiao, K., Berti, L., Luo, J., Tseng, H. P., Fung, G., and Lam, K. S. (2012) Well-defined, reversible boronate crosslinked nanocarriers for targeted drug delivery in response to acidic ph values and cis-diols. *Angew. Chem. Int. Ed. 51*, 2864-2869.
(22) Kennedy, L. C., Bickford, L. R., Lewinski, N. A., Coughlin, A. J., Hu, Y., Day, E. S., West, J. L., and Drezek, R. A. (2011) A new era for cancer treatment: Gold-nanoparticle-mediated thermal therapies. *Small 7*, 169-83.

(23) Shanmugam, V., Selvakumar, S., and Yeh, C. S. (2014) Near-infrared light-responsive nanomaterials in cancer therapeutics. *Chem. Soc. Rev. 43*, 6254-87.
(24) Bhattacharyya, S., Gonzalez, M., Robertson, J. D., Bhattacharya, R., and Mukherjee, P. (2011) A simple synthesis of a targeted drug delivery system with enhanced cytotoxicity. *Chem. Commun. (Camb.) 47*, 8530-2.
(25) Shanmugam, V., Chien, Y. H., Cheng, Y. S., Liu, T. Y., Huang, C. C., Su, C. H., Chen, Y. S., Kumar, U., Hsu, H. F., and Yeh, C. S. (2014) Oligonucleotides--assembled au nanorod-assisted cancer photothermal ablation and combination chemotherapy with targeted dual-drug delivery of doxorubicin and cisplatin prodrug. *ACS Appl. Mater. Interfaces 6*, 4382-93.
(26) Sun, T., Zhang, Y. S., Pang, B., Hyun, D. C., Yang, M., and Xia, Y. (2014) Engineered nanoparticles for drug delivery in cancer therapy. *Angew. Chem. Int. Ed. 53*, 12320-64.
(27) Eck, W., Craig, G., Sigdel, A., Ritter, G., Old, L. J., Tang, L., Brennan, M. F., Allen, P. J., and Mason, M. D. (2008) Pegylated gold nanoparticles conjugated to monoclonal f19 antibodies as targeted labeling agents for human pancreatic carcinoma tissue. *ACS Nano 2*, 2263-2272.
(28) Chen, Y., Li, N., Yang, Y., and Liu, Y. (2015) A dual targeting cyclodextrin/gold nanoparticle conjugate as a scaffold for solubilization and delivery of paclitaxel. *RSC Adv 5*, 8938-8941.
(29) Brown, S. D., Nativo, P., Smith, J.-A., Stirling, D., Edwards, P. R., Venugopal, B., Flint, D. J., Plumb, J. A., Graham, D., and Wheate, N. J. (2010) Gold nanoparticles for the improved anticancer drug delivery of the active component of oxaliplatin. *J. Am. Chem. Soc. 132*, 4678-4684.
(30) Paciotti, G. F., Myer, L., Weinreich, D., Goia, D., Pavel, N., McLaughlin, R. E., and Tamarkin, L. (2004) Colloidal gold: A novel nanoparticle vector for tumor directed drug delivery. *Drug delivery 11*, 169-83.
(31) Kasten, B. B., Liu, T., Nedrow-Byers, J. R., Benny, P. D., and Berkman, C. E. (2013) Targeting prostate cancer cells with psma inhibitor-guided gold nanoparticles. *Bioorg. Med. Chem. Lett. 23*, 565-8.
(32) Coelho, S. C., Rocha, S., Pereira, M. C., Juzenas, P., and Coelho, M. A. N. (2014) Enhancing proteasome-inhibitor effect by functionalized gold nanoparticles. *J. Biomed. Nanotechnol. 10*, 717-723.
(33) He, C., Lu, J., and Lin, W. (2015) Hybrid nanoparticles for combination therapy of cancer. *J. Control Release 219*, 224-36.
(34) Paterson, B. M., and Donnelly, P. S. (2011) Copper complexes of bis(thiosemicarbazones): From chemotherapeutics to diagnostic and therapeutic radiopharmaceuticals. *Chem. Soc. Rev. 40*, 3005-18.
(35) L. J. Dearling, J., and J. Blower, P. (1998) Redox-active metal complexes for imaging hypoxic tissues: Structure-activity relationships in copper(ii) bis(thiosemicarbazone) complexes. *Chem. Commun.*, 2531-2532.
(36) Luo, T., Yu, J., Nguyen, J., Wang, C.-R., Bristow, R. G., Jaffray, D. A., Zhou, X. Z., Lu, K. P., and Lu, Q.-B. (2012) Electron transfer-based combination therapy of cisplatin with tetramethyl-p-phenylenediamine for ovarian, cervical, and lung cancers. *Proc. Natl. Acad. Sci. U.S.A. 109*, 10175-10180.
(37) Palanimuthu, D., Shinde, S. V., Somasundaram, K., and Samuelson, A. G. (2013) In vitro and in vivo anticancer activity of copper bis(thiosemicarbazone) complexes. *J. Med. Chem. 56*, 722-34.
(38) Stefani, C., Al-Eisawi, Z., Jansson, P. J., Kalinowski, D. S., and Richardson, D. R. (2015) Identification of differential anti-neoplastic activity of copper bis(thiosemicarbazones) that is mediated by intracellular reactive oxygen species generation and lysosomal membrane permeabilization. *J. Inorg. Biochem. 152*, 20-37.
(39) Helsel, M. E., and Franz, K. J. (2015) Pharmacological activity of metal binding agents that alter copper bioavailability. *Dalton Trans. 44*, 8760-70.

(40) Dearling, J. L., Lewis, J. S., Mullen, G. E., Welch, M. J., and Blower, P. J. (2014) Copper bis(thiosemicarbazone) complexes as hypoxia imaging agents: Structure-activity relationships. *J. Biol. Inorg. Chem. 7*, 249-259.

(41) Bonnitcha, P. D., Vāvere, A. L., Lewis, J. S., and Dilworth, J. R. (2008) In vitro and in vivo evaluation of bifunctional bisthiosemicarbazone 64cu-complexes for the positron emission tomography imaging of hypoxia. *J. Med. Chem. 51*, 2985-2991.

(42) Kobayashi, H., Watanabe, R., and Choyke, P. L. (2013) Improving conventional enhanced permeability and retention (epr) effects; what is the appropriate target? *Theranostics 4*, 81-9.

(43) Lee, M. H., Sessler, J. L., and Kim, J. S. (2015) Disulfide-based multifunctional conjugates for targeted theranostic drug delivery. *Acc. Chem. Res. 48*, 2935-46.

(44) Christlieb, M., Struthers, H. S., Bonnitcha, P. D., Cowley, A. R., and Dilworth, J. R. (2007) The exocyclic functionalisation of bis(thiosemicarbazonate) complexes of zinc and copper: The synthesis of monomeric and dimeric species. *Dalton Trans.*, 5043-54.

(45) Roux, S., Garcia, B., Bridot, J.-L., Salomé, M., Marquette, C., Lemelle, L., Gillet, P., Blum, L., Perriat, P., and Tillement, O. (2005) Synthesis, characterization of dihydrolipoic acid capped gold nanoparticles, and functionalization by the electroluminescent luminol. *Langmuir 21*, 2526-2536.

(46) Liu, W., Howarth, M., Greytak, A. B., Zheng, Y., Nocera, D. G., Ting, A. Y., and Bawendi, M. G. (2008) Compact biocompatible quantum dots functionalized for cellular imaging. *J. Am. Chem. Soc. 130*, 1274-1284.

(47) Susumu, K., Oh, E., Delehanty, J. B., Blanco-Canosa, J. B., Johnson, B. J., Jain, V., Hervey, W. J. t., Algar, W. R., Boeneman, K., Dawson, P. E., et al. (2011) Multifunctional compact zwitterionic ligands for preparing robust biocompatible semiconductor quantum dots and gold nanoparticles. *J. Am. Chem. Soc. 133*, 9480-96.

(48) Turkevich, J., Stevenson, P. C., and Hillier, J. (1951) A study of the nucleation and growth processes in the synthesis of colloidal gold. *Faraday Discuss. 11*, 55.

(49) Frens, G. (1973) Controlled nucleation for the regulation of the particle size in monodisperse gold suspensions. *Nat. Phys. Sci. 241*, 20-22.

(50) Kumar, D., Meenan, B. J., and Dixon, D. (2012) Glutathione-mediated release of bodipy(r) from peg cofunctionalized gold nanoparticles. *Int. J. Nanomedicine 7*, 4007-22.

(51) Plażuk, D., Zakrzewski, J., Salmain, M., Błauż, A., Rychlik, B., Strzelczyk, P., Bujacz, A., and Bujacz, G. (2013) Ferrocene–biotin conjugates targeting cancer cells: Synthesis, interaction with avidin, cytotoxic properties and the crystal structure of the complex of avidin with a biotin–linker–ferrocene conjugate. *Organometallics 32*, 5774-5783.

(52) Craig, G. E., Brown, S. D., Lamprou, D. A., Graham, D., and Wheate, N. J. (2012) Cisplatin-tethered gold nanoparticles that exhibit enhanced reproducibility, drug loading, and stability: A step closer to pharmaceutical approval? *Inorg. Chem. 51*, 3490-7.

(53) Ducry, L., and Stump, B. (2010) Antibody−drug conjugates: Linking cytotoxic payloads to monoclonal antibodies. *Bioconjugate Chem. 21*, 5-13.

(54) Dhar, S., Reddy, E. M., Shiras, A., Pokharkar, V., and Prasad, B. L. V. (2008) Natural gum reduced/stabilized gold nanoparticles for drug delivery formulations. *Chem. Eur. J. 14*, 10244-10250.

(55) Valerio, V., Giovanni, S., Riccardo, N., Fernanda, R., Stefano, L., and Fabio, B. (2012) Smart delivery and controlled drug release with gold nanoparticles: New frontiers in nanomedicine. *Recent Pat. Nanomed. 2*, 34-44.

(56) Montero, D., Tachibana, C., Rahr Winther, J., and Appenzeller-Herzog, C. (2013) Intracellular glutathione pools are heterogeneously concentrated. *Redox Biol. 1*, 508-13.

(57) Ren, T., Wu, W., Jia, M., Dong, H., Li, Y., and Ou, Z. (2013) Reduction-cleavable polymeric vesicles with efficient glutathione-mediated drug release behavior for reversing drug resistance. *ACS Appl. Mater. Interfaces 5*, 10721-30.

(58) Russo, A., DeGraff, W., Friedman, N., and Mitchell, J. B. (1986) Selective modulation of glutathione levels in human normal versus tumor cells and subsequent differential response to chemotherapy drugs. *Cancer Res. 46*, 2845.

(59) Yin, T., Wu, Q., Wang, L., Yin, L., Zhou, J., and Huo, M. (2015) Well-defined redox-sensitive polyethene glycol-paclitaxel prodrug conjugate for tumor-specific delivery of paclitaxel using octreotide for tumor targeting. *Mol. Pharm. 12*, 3020-31.

(60) Fang, J., Nakamura, H., and Maeda, H. (2011) The epr effect: Unique features of tumor blood vessels for drug delivery, factors involved, and limitations and augmentation of the effect. *Adv. Drug Deliv. Rev. 63*, 136-51.

(61) Dharmarajan, N. M. a. T. S. (2002) Synthesis, characterization and biological activity of copper(ii) complexes with phenylglyoxal bis(thiosemicarbazone). *Asian J. Chem. 14*, 1325−1330.

(62) Price, K. A., Caragounis, A., Paterson, B. M., Filiz, G., Volitakis, I., Masters, C. L., Barnham, K. J., Donnelly, P. S., Crouch, P. J., and White, A. R. (2009) Sustained activation of glial cell epidermal growth factor receptor by bis(thiosemicarbazonato) metal complexes is associated with inhibition of protein tyrosine phosphatase activity. *J. Med. Chem. 52*, 6606-20.

(63) Xiao, Z., Donnelly, P. S., Zimmermann, M., and Wedd, A. G. (2008) Transfer of copper between bis(thiosemicarbazone) ligands and intracellular copper-binding proteins. Insights into mechanisms of copper uptake and hypoxia selectivity. *Inorg. Chem. 47*, 4338-4347.

(64) Ren, W. X., Han, J., Uhm, S., Jang, Y. J., Kang, C., Kim, J.-H., and Kim, J. S. (2015) Recent development of biotin conjugation in biological imaging, sensing, and target delivery. *Chem. Commun. 51*, 10403-10418.

(65) Heo, D. N., Yang, D. H., Moon, H. J., Lee, J. B., Bae, M. S., Lee, S. C., Lee, W. J., Sun, I. C., and Kwon, I. K. (2012) Gold nanoparticles surface-functionalized with paclitaxel drug and biotin receptor as theranostic agents for cancer therapy. *Biomaterials 33*, 856-66.

(66) Yang, W., Cheng, Y., Xu, T., Wang, X., and Wen, L. P. (2009) Targeting cancer cells with biotin-dendrimer conjugates. *Eur. J. Med. Chem. 44*, 862-8.

(67) Kai, M. P., Keeler, A. W., Perry, J. L., Reuter, K. G., Luft, J. C., O'Neal, S. K., Zamboni, W. C., and DeSimone, J. M. (2015) Evaluation of drug loading, pharmacokinetic behavior, and toxicity of a cisplatin-containing hydrogel nanoparticle. *J. Control Release 204*, 70-7.

(68) Quintana, A., Raczka, E., Piehler, L., Lee, I., Myc, A., Majoros, I., Patri, A. K., Thomas, T., Mulé, J., and Baker, J. R. Design and function of a dendrimer-based therapeutic nanodevice targeted to tumor cells through the folate receptor. *Pharm. Res. 19*, 1310-1316.

(69) Guo, S., Lv, L., Shen, Y., Hu, Z., He, Q., and Chen, X. (2016) A nanoparticulate pre-chemosensitizer for efficacious chemotherapy of multidrug resistant breast cancer. *Sci. Rep. 6*, 21459.

(70) Patil, Y., Sadhukha, T., Ma, L., and Panyam, J. (2009) Nanoparticle-mediated simultaneous and targeted delivery of paclitaxel and tariquidar overcomes tumor drug resistance. *J. Controlled Release 136*, 21-29.

(71) Patil, Y. B., Toti, U. S., Khdair, A., Ma, L., and Panyam, J. (2009) Single-step surface functionalization of polymeric nanoparticles for targeted drug delivery. *Biomaterials 30*, 859-866.

(72) Patil, Y. B., Swaminathan, S. K., Sadhukha, T., Ma, L., and Panyam, J. (2010) The use of nanoparticle-mediated targeted gene silencing and drug delivery to overcome tumor drug resistance. *Biomaterials 31*, 358-365.

(73) Taheri, A., Dinarvand, R., Nouri, F. S., Khorramizadeh, M. R., Borougeni, A. T., Mansoori, P., and Atyabi, F. (2011) Use of biotin targeted methotrexate-human serum albumin conjugated nanoparticles to enhance methotrexate antitumor efficacy. *Int. J. Nanomedicine 6*, 1863-74.

(74) Das, S., and Somasundaram, K. (2006) Therapeutic potential of an adenovirus expressing p73beta, a p53 homologue, against human papilloma virus positive cervical cancer in vitro and in vivo. *Cancer Biol. Ther. 5*, 210-217.

(75) Chen, L., Xue, Y., Xia, X., Song, M., Huang, J., Zhang, H., Yu, B., Long, S., Liu, Y., Liu, L., et al. (2015) A redox stimuli-responsive superparamagnetic nanogel with chemically anchored dox for enhanced anticancer efficacy and low systemic adverse effects. *J. Mater. Chem. B 3*, 8949-8962.

(76) Holland, J. P., Aigbirhio, F. I., Betts, H. M., Bonnitcha, P. D., Burke, P., Christlieb, M., Churchill, G. C., Cowley, A. R., Dilworth, J. R., Donnelly, P. S., et al. (2007) Functionalized bis(thiosemicarbazonato) complexes of zinc and copper: Synthetic platforms toward site-specific radiopharmaceuticals. *Inorg. Chem. 46*, 465-485.

(77) Wu, Y. L., and Li, J. (2009) Synthesis of supramolecular nanocapsules based on threading of multiple cyclodextrins over polymers on gold nanoparticles. *Angew. Chem. Int. Ed. 48*, 3842-5.

(78) Susumu, K., Mei, B. C., and Mattoussi, H. (2009) Multifunctional ligands based on dihydrolipoic acid and polyethylene glycol to promote biocompatibility of quantum dots. *Nat. Protoc. 4*, 424-36.

(79) Qi, K., Ma, Q., Remsen, E. E., Clark, C. G., and Wooley, K. L. (2004) Determination of the bioavailability of biotin conjugated onto shell cross-linked (sck) nanoparticles. *J. Am. Chem. Soc. 126*, 6599-6607.

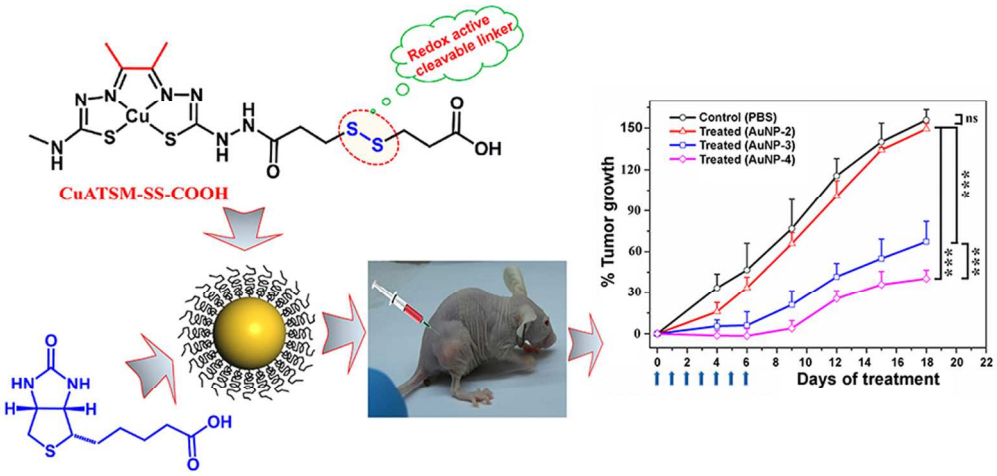

85x40mm (300 x 300 DPI)